Attenuation correction for dedicated breast PET using only emission data based on consistency conditions*

WANG Lu(王璐)[1,2] CHAI Pei(柴培)[1] WU Li-Wei(武丽伟)[1,2] YUN Ming-Kai(员明凯)[1]
ZHOU Xiao-Lin(周小林)[1,2] LIU Shuang-Quan(刘双全)[3] ZHANG Yu-Bao(张玉包)[3]
SHAN Bao-Ci(单保慈)[1;1)] WEI Long(魏龙)[1,3]

[1] Key Laboratory of Nuclear Analysis Techniques, Institute of High Energy Physics, Chinese Academy of Sciences, Beijing 100049, China
[2] Graduate University of Chinese Academy of Sciences, Beijing 100049, China
[3] Beijing Engineering Research Center of Radiographic Techniques and Equipment, Beijing 100049, China

Abstract: Accurate attenuation correction is required in dedicated breast PET imaging systems for image artifact removal and quantitative studies. In this study, a method using only emission data based on consistency conditions is proposed for attenuation correction in breast PET imaging systems. The consistency conditions are exploited to evaluate the accuracy of the estimated attenuation distribution and find the appropriate parameters that yield the most consistent attenuation distribution with the measured emission data. We have proved the validity of the method with experimental investigations and single-patient studies using a dedicated breast PET. The results show that the method is capable of accurately estimating the attenuation distribution of a uniform attenuator from the experimental data with various relatively low activities. The results also show that in single-patient studies, the method is robust for the irregular boundary of breast tissue and provides a distinct improvement in image quality.

Key words: attenuation correction, breast PET, consistency conditions

PACS: 87.55.k-, 87.57.uk, 87.57.C- **DOI:** 10.1088/1674-1137/37/1/018201

1 Introduction

Dedicated breast positron emission tomography (PET) is a noninvasive imaging method for primary breast tumor detection [1–3]. Compared with whole-body PET, it can offer better perspectives in terms of resolution and detection sensitivity to improve the diagnostic accuracy of breast cancer with small lesions and low lesion-to-background ratio [4, 5].

Accurate attenuation correction is required in dedicated breast PET imaging systems for image artifact removal and quantitative studies. The accuracy achieved by the attenuation correction methods depends mainly on the rigor followed to derive the reliable attenuation distribution, which relies on accurate delineation of the tissue boundary and often necessitates knowledge of the anatomic structure and some transmission information [6]. A current trend in PET is to use the supplementary acquisition of the transmission scans to obtain the attenuation distribution [7–9], which considerably increases the additional radiation dose and complicates the system design and the protocols of the data acquisition and processing for dedicated breast PET.

In some cases, the attenuation distribution can be acquired by using only the emission data in the absence of the transmission scans, such as employing limited transmission information from the emission data and segmenting the emission data into different regions with the assumption that each region has its own attenuation coefficient and the attenuation distribution within each region is uniform [10–12]. These methods have been shown to yield good results in a number of situations but still suffer from the drawback that in general the segmentation thresholds are difficult to define from the emission data without adequate transmission information, especially when the activity ratios between the different regions are relatively low. Furthermore, these methods produce little evidence to support that the attenuation distribution acquired by the segmentation based on limited transmission information from the emission data is consistent with the true attenuation distribution from the emission data.

Until recently, more dramatic advancements in transmissionless techniques have been investigated with the

Received 28 February 2012, Revised 15 May 2012
* Supported by National Natural Science Foundation of China (81101070)
1) E-mail: shanbc@ihep.ac.cn

aim of reconstructing the attenuation distribution directly from the emission data without any transmission measurements but with some principles of mathematics linking the attenuation distribution with the attenuated emission data. Among these, the methods based on the data consistency conditions have attracted more attention. The consistency conditions are composed of a set of equations relating the attenuated emission data and the corresponding transmission sinogram. By solving these equations, the attenuation distribution which is most consistent with the emission data can be estimated directly from the measured emission data. However, the problem is highly underdetermined because few equations can be invoked in practice. Therefore, it is necessary to reduce the complexity of the problem to use some prior information of the attenuation distribution and narrow the search space of the consistency conditions [13–16].

In this study, we proposed a method based on the consistency conditions for the attenuation correction in breast PET imaging systems. Considering that the contour of the human breast is convex and moreover the anatomic structure is simple [10], we perform the segmentation between the breast tissue and the background region in the projection space of the measured emission data. After projecting back the segmented emission sinograms, the known attenuation coefficients are assigned to the two regions in the image space, and the initial attenuation distribution is generated as the prior information of the consistency conditions. The key point of this method is that the consistency conditions are exploited to evaluate the accuracy of the segmentation and find the appropriate thresholds as the segmentation parameters that yield the most consistent attenuation distribution with the emission data. We have proved the validity of the proposed method with experimental investigations and single-patient studies using a dedicated breast PET(PEMi, Institute of High Energy Physics, Chinese Academy of Sciences) [17].

2 Theory

The consistency conditions are a set of mathematical rules derived from the Radon transform that should be satisfied by perfect PET data, such as the attenuation-corrected data. Eq. (1) gives Natterer's formulation of the Helgason-Ludwig consistency conditions for the PET data [18, 19]

$$\int_0^{2\pi}\int_{-\infty}^{\infty} s^m \mathrm{e}^{\mathrm{i}k\phi}\mathrm{e}^{T(s,\phi)}E(s,\phi)\mathrm{d}s\mathrm{d}\phi=0, \qquad (1)$$

where s is the radial distance from the center of the rotation in the Radon transform space; ϕ is the azimuthal angle of the rotation in the Radon transform space; $E(s,\phi)$ is the measured emission data; $T(s,\phi)$is the Radon transform of the attenuation distribution; m is an integer greater than or equal to zero and determines which moment is being calculated; and k is an integer greater than m or $k+m$ is odd and determines which is the Fourier component.

In Eq. (1), with the given emission data $E(s,\phi)$, which are obtained by a PET system, the attenuation distribution can be calculated by solving the above equations of the consistency conditions. In practice, the non-linear system is highly underdetermined because few equations can be invoked. Furthermore, due to the errors introduced by noise, discretization errors and other physical factors, the problem is ill-posed, causing the objective function to have too many local minima.

However, if we can parameterize the attenuation distribution in some way by using some prior information, we can reduce the complexity of the problem and narrow the search space of the consistency conditions. For the work presented here it is assumed that the boundary of the breast tissue is convex, and the anatomic structure is simple [10]. We perform the segmentation between different tissues or regions in the projection space of the measured emission data, and after projecting back the segmented emission sinograms, the known attenuation coefficients are assigned to the different regions in the image space, and the initial attenuation distribution is generated as the prior information of the consistency conditions. As a result, the segmentation thresholds for those regions are introduced as a reasonable number of parameters to parameterize the attenuation distribution, we can use the consistency conditions to estimate these parameters.

In this study, the emission sinograms are segmented into the breast tissue and the background region. Therefore, only one segmentation threshold is estimated, referred to as T. The attenuation coefficient for the background region is taken to be zero, and the attenuation coefficient is assigned to be 0.0098 mm^{-1} for the breast tissue [20].

The consistency conditions are exploited as a measure of estimation accuracy of the attenuation distribution with the current segmentation threshold. If the attenuation distribution is not consistent with the measured emission data, Eq. (1) will be nonzero in different values of m and k [15, 21]. Therefore, these equations are summed to measure the consistency of the estimated attenuation distribution and the measured emission data, then the segmentation threshold can be obtained and optimized by minimizing the following objective function:

$$F_{m,k}=\sum_{0\leqslant m<k}\left\|\int_0^{2\pi}\int_{-\infty}^{\infty} s^m \mathrm{e}^{\mathrm{i}k\phi}\mathrm{e}^{T(s,\phi)}E(s,\phi)\mathrm{d}s\mathrm{d}\phi\right\|^2. \qquad (2)$$

The Levenberg-Marquardt algorithm [22] is used to find the optimal segmentation threshold. At each it-

eration, the emission sinogram is segmented using the current estimation of the segmentation threshold, and the updated attenuation distribution is formed when the known attenuation coefficients are assigned to the two regions in the image space after projecting back the segmented emission sinogram. And then the updated attenuation distribution is projected to provide the attenuation transmission sinogram used in (2). The objective function is produced by evaluating (2) for certain values of m and k and summing the results. In this study, we use the values of 1 and 2 for m and the values of k such that $m<k<9$ and $k+m$ is odd. The stopping rule for the algorithm is that there is less than 0.1% change in the objective function with no other penalties.

3 Methods and results

3.1 Experimental investigations

A uniformly attenuating cylindrical phantom was designed to test whether the proposed method could determine the boundary of a uniform attenuator from experimental data and remove the image artifacts. The phantom was a hollow cylinder with 158.0 mm in length and 100.0 mm in diameter, which was filled with 18F-FDG solution having activity concentration of 200 nCi/cm^3, as a typical 18F-FDG uptake value of breast tissue [23]. The phantom was placed in the center of the FOV, and then was scanned by the PEMi.

The emission data were binned into a 127×256×127 projection array, which represented that 127 sinogram planes were acquired and 127 radial bins and 256 angles were sampled for each sinogram plane. After corrections for random, normalization, dead time and scatter, the images were reconstructed using the ordered subsets expectation maximization maximum-likelihood method (OSEM) [24] with two iterations and eight subsets in these three cases: in the first one, no correction was performed for attenuation; in the second one, the attenuation correction was performed using the true attenuation distribution; in the third one, the attenuation correction was performed using the estimated attenuation distribution from the proposed method with the attenuation coefficient of 0.0096 mm^{-1} for the water [20] and the initial threshold of 10% of the maximum counts over all the radial bins of each angle in the sinogram plane.

The estimated boundaries and the reconstructed images from a typical transaxial slice of the phantom are shown in Fig. 1. The results in Fig. 1 (a) show that, though the phantom has been filled with the uniform 18F-FDG solution, the central region of the reconstructed image appears to be lighter than the outer and the contrast artifacts between them are distinct. That is because the emission photons from the central region of the phantom are in more loss of quantity than the outer by reason that the central photons go a longer way in the attenuator. However, the results in Fig.1 (b), (c) and (d) show that the proposed method is capable of accurately estimating the boundary of a uniform attenuator from experimental data and eliminating the contrast artifacts just as the method using the true attenuation distribution does.

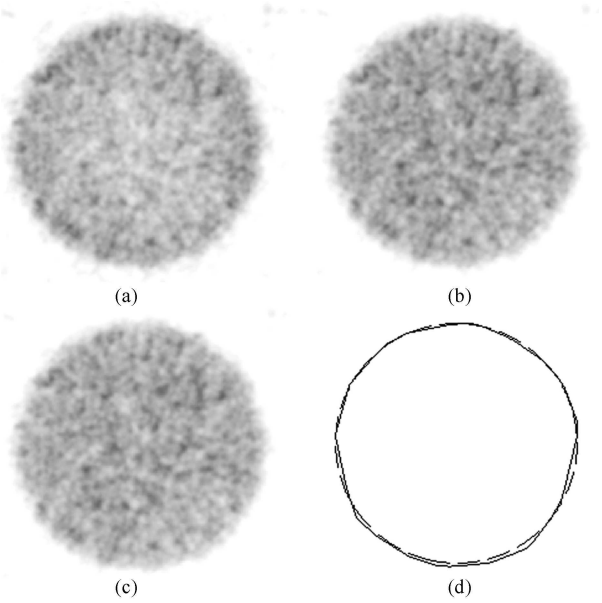

Fig. 1. The reconstructed images from the typical slice of the cylindrical phantom with the activity concentration of 200 nCi/cm^3 performed by: (a) no attenuation correction, (b) the attenuation correction using the true attenuation distribution and (c) the estimated attenuation distribution from the proposed method. (d) the boundaries of the true attenuation distribution (dashed line) and the estimated attenuation distribution from the proposed method (solid line).

In order to quantitatively evaluate the results of the attenuation correction mentioned above, nine 10-mm width concentric annular regions of interest (ROI) are defined, which are referred to as numbers 1 to 9 from the outer to the center of the images. These ROIs are completely within and not close to the edge of the phantom to avoid partial volume edge effects.

Figure 2 shows the mean values of the pixels in each ROI before attenuation correction, the attenuation correction using the true attenuator, and using the estimated attenuator from the proposed method, respectively. The results show that attenuation can introduce the contrast artifacts which cause the mean profile drops as the depth of the ROI increases in uncorrected images. Nevertheless, the artifacts are reduced effectively when the attenuation correction is performed by either the true attenuator or the estimated attenuator using the

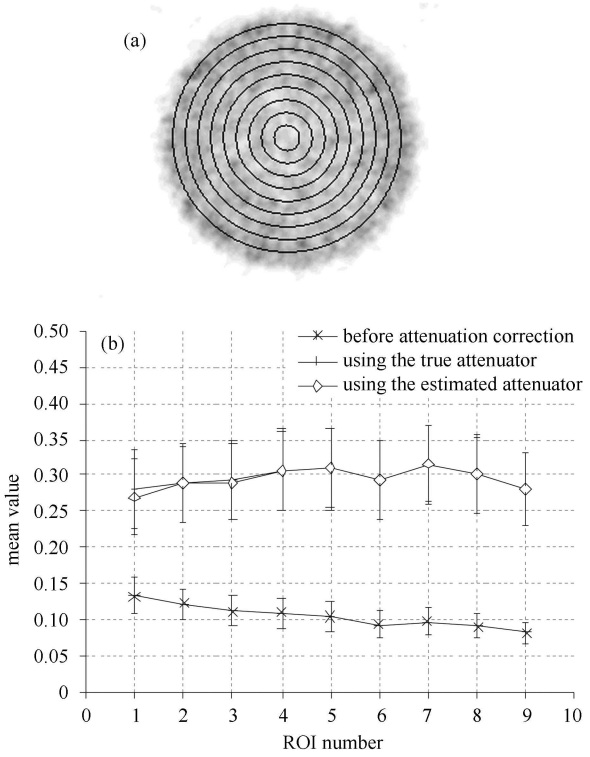

Fig. 2. The quantitative analysis of the reconstructed images in Fig. 1: (a) the ROIs details and (b) the quantitative performance for no attenuation correction, the attenuation correction using the true attenuator, and the attenuation correction using the estimated attenuator from the proposed method, respectively.

proposed method. The results also show that after attenuation correction, the mean values of the pixels increase but the non-uniformity from the original images are more distinct because the standard deviation variances between the pixels are also magnified. We suppose that the key challenge comes from relatively low activity, which causes low statistics and poor signal-to-noise ratio. Moreover, we should consider other effects such as the uniformity from the imaging system in practice, and the accuracy of normalization correction.

In order to investigate the robustness of the proposed method with various relatively low activities, another two sets of experimental data were acquired with the activity concentrations of 100 nCi/cm^3 and 50 nCi/cm^3, respectively. Compared with the case of the activity concentration of 200 nCi/cm^3, the acquisition and reconstruction of the two sets were accomplished in the same way.

The estimated boundaries and the reconstructed images from a typical transaxial slice of the phantom are shown in Fig. 3. In each set, the results show that the attenuation correction based on the estimated attenuation distribution using the proposed method can produce reconstructed images which are considerably closer to those corrected using the true attenuation distribution, though the estimated boundaries are slightly inconsistent with the true boundaries. Therefore, we would expect that the proposed method would be robust for different relatively low activities and offer an appropriate correction for a uniform attenuator.

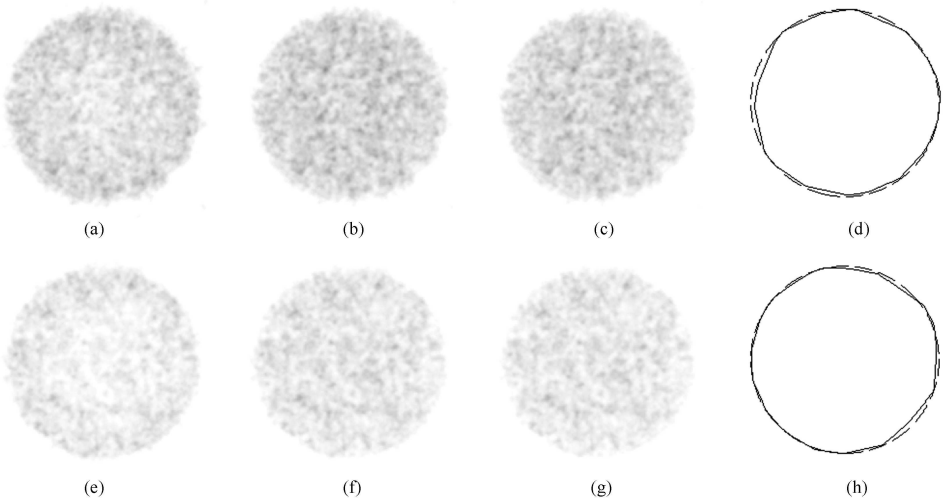

Fig. 3. The reconstructed images from a typical slice of the cylindrical phantom with the activity concentrations of 100 nCi/cm^3 (shown in (a) to (d)) and 50 nCi/cm^3 (shown in (e) to (h)) performed by: (a) and (e) no attenuation correction, (b) and (f) the attenuation correction using the true attenuation distribution, and (c) and (g) the estimated attenuation distribution from the proposed method. (d) and (h) the boundaries of the true attenuation distribution (the dashed line) and the estimated attenuation distribution from the proposed method (the solid line).

3.2 Single-patient studies

To explore the validity of the proposed method in clinical practice, we tested the method with two sets of patient data from the PEMi. After correcting all physical effects (random, normalization, dead time and scatter) except attenuation, the data from the patients were reconstructed using the OSEM method in two iterations and eight subsets in these two cases: in one case, attenuation correction was not performed; and in the other case, the attenuation correction was performed using the proposed method with the attenuation coefficient of 0.0098 mm^{-1} for the breast tissue and the initial threshold of 10%.

The reconstructed images from the patients are shown in Fig. 4. The results show that the proposed method is robust for the irregular boundary of the breast tissue, and the attenuation correction can suppress the noise and reduce the artifacts in the reconstructed images. Furthermore, the results also show that after attenuation correction, the image contrast between the central region and the outer region of the breast tissue could be improved, which is helpful for diagnosis of lesions, especially when the lesions are located in the center of the upper slices of the breast where the photons encounter more serious attenuation.

4 Discussion and conclusion

The results of the experimental investigations for the cylindrical phantom show that the proposed method can accurately estimate the attenuation distribution from a uniform attenuator with different activities. The results also suggest that the success of the method does not depend on the statistics too. However, a more thorough analysis is required to determine whether the results of the method have any dependence on relatively good statistics.

Supposing there is a sudden situation that most of the activity distribution is concentrated in the cancer lesions but little is concentrated in other regions, it is impossible to segment between the breast tissue and the background region and derive the boundary information

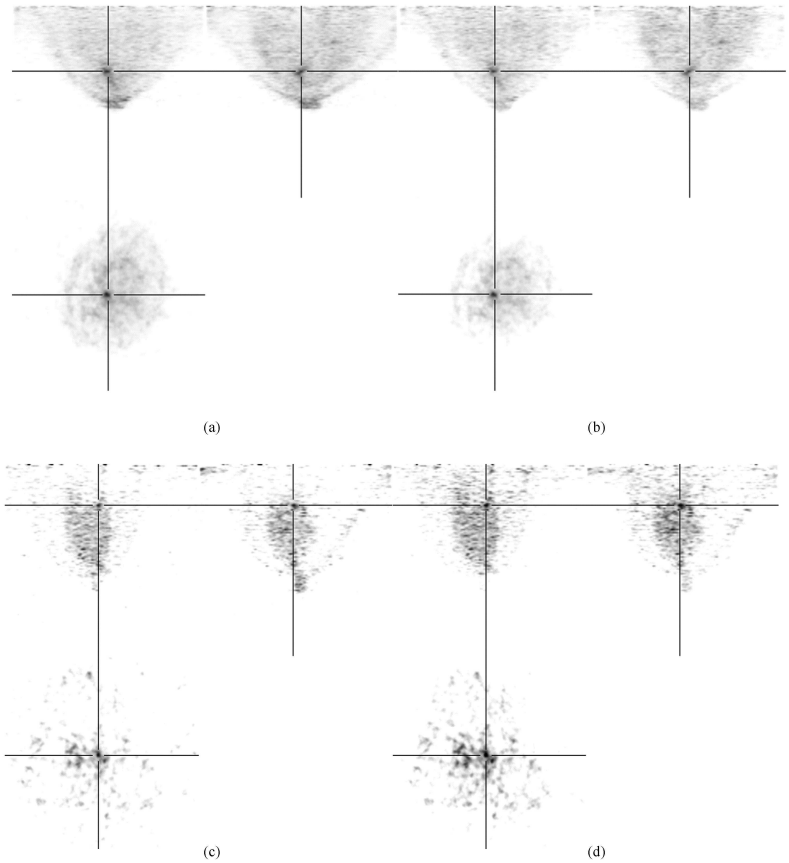

Fig. 4. The reconstructed images from Patient A (shown in (a) and (b)) and Patient B (shown in (c) and (d)), performed by: (a) and (c) no attenuation correction, (b) and (d) the attenuation correction using the proposed method.

from the emission data even if the consistency conditions are employed. That is, the proposed method does not work. However, in practice, the absorption of the radiopharmaceuticals by the normal breast tissue is not zero but a smaller amount compared with the concentrated areas, as shown in Fig. 4, and therefore false cases rarely occur.

In quantitative studies, the results suggest that attenuation correction might magnify the non-uniformity from the original images. For breast PET imaging systems, relatively low activity would bring the key challenge, which could cause low statistics and a poor signal-to-noise ratio. In addition, the uniformity from the imaging system and the accuracy of normalization correction should considered.

The results of the patient studies verify that the proposed method is relatively insensitive to the boundary perturbations in the attenuation distribution, such as the irregular shapes. The results also show that attenuation can introduce contrast artifacts into reconstructed images. Therefore, in order to suppress noise and reduce artifacts, attenuation correction is required in breast PET imaging systems, especially for lesions located in places where photons encounter more serious attenuation.

In conclusion, we have shown that a method based on the consistency conditions is an efficient attenuation correction method for estimating the boundary of a uniform attenuator from the emission data measured by the PEMi. We have tested the method using the experimental data, and as it stands, the method can be of clinical use for patient studies.

However, as shown in Fig. 4, it is interesting to note that human breast tissue is not uniform and some investigations [25–27] also support the fact that breast tissue can be segmented into two parts with different attenuation coefficients and absorption of radiopharmaceuticals, such as the fat tissue and the gland tissue. Nevertheless, experimental investigations in dedicated breast SPECT indicate that the differences in the attenuation between materials do not affect the quantification as much as the size of the attenuation distribution. Thus Perez et al suppose that the assumption of the attenuator could be sufficient for quantitative studies in breast SPECT imaging systems [28].

Our future work will focus on testing the proposed method using a wider range of clinical data in order to ascertain whether the approximation of the uniform attenuation distribution of the breast tissue is robust. Furthermore, we will investigate the necessity that the attenuation correction should be concerned about compensating for non-uniform attenuation and segmenting the breast tissue into the fat and gland tissue in breast PET imaging systems.

References

1 Raylman R R, Majewski S, Wojcik R et al. Medical Physics, 2000, **24**: 1943
2 Berg W A, Weinberg I N, Narayanan D et al. The Breast Journal, 2006, **12**: 309
3 Abreu M, Aguiar D, Albuquerque E et al. Nuclear Instruments and Methods in Physics Research, A, 2007, **571**: 81
4 Avril N, Schelling M, Dose J et al. Journal of Clinical Oncology, 2000, **18**: 3495
5 WU Y, YANG K, Packard N et al. Physics in Medicine and Biology, 2009, **54**: 4273
6 Zaidi H and Hasegawa B. Journal of Nuclear Medicine, 2003, **44**: 291
7 Bailey D L. European Journal of Nuclear Medicine and Molecular Imaging, 1998, **25**: 774
8 Kinahan P, Townsend D W, Beyer T et al. Medical Physics, 1998, **25**: 2046
9 Beyer T, Townsend D W, Brun T et al. Journal of Nuclear Medicine, 2000, **41**: 1369
10 Soriano A, Gonzálezb A, Orero A et al. NIMA_4th International Conference on Imaging Techniques in Subatomic Physics. Astrophysics, Medicine: Biology and Industry, 2010, **648**: S75
11 Wallis J W, Miller T R, Koppel P et al. Journal of Nuclear Medicine, 1995, **36**: 506
12 Hebert T J, Gopal S S, Murphy P. IEEE Transactions on Medical Imaging, 1995, **14**: 22
13 Natterer F. Inverse Problems, 1993, **9**: 731
14 Panin V Y, Clack R, Natterer F et al. Journal of Nuclear Medicine, 1998,**39**: 799
15 Laurette I, Clackdoyle R, Welch A et al. IEEE Transactions on Nuclear Science, 1999, **46**: 2146
16 Welch A, Campbell C, Clackdoyle R et al. 1997 IEEE Nuclear Science Symposium Conference Record, 1997. 1697
17 YAN Q, GAO J, SHAN B C et al. Chinese Physics C (HEP & NP), 2010, **34**: 152
18 Natterer F. The Mathematics of Computerized Tomography. Philadelphia. Pennsylvania: Society for Industrial Mathematics, 2001. 46
19 JIN Y J, MA T Y. Nuclear Medical Instrument and Method. Harbin: Harbin Engineering University Press, 2010. 117–119
20 http://www.nist.gov/pml/data/xraycoef/index.cfm
21 Bromiley A, Welch A, Chilcottet F et al. IEEE Transactions on Nuclear Science, 2002, **48**: 1371–1377
22 Marquardt D W. Journal of the Society for Industrial and Applied Mathematics, 1963, **11**: 431
23 Trindade A, Almeida P, Balau F et al. 2003 IEEE Nuclear Science Symposium Conference Record, 2003, **3**: 1918
24 Hudson H M, Larkin R S. IEEE Transactions on Medical Imaging, 1994, **13**: 601
25 Byng J, Mainprize J G, Yaffe M J. Physics in Medicine and Biology, 1998, **43**: 1367
26 Guimarães L T G, Schiabel H, Stemberg D R M. World Congress on Medical Physics and Biomedical Engineering, 2009, **25**: 454
27 CHEN R C, Longo R, Rigon L et al. Physics in Medicine and Biology, 2010, **55**: 4993
28 Perez K L, Mann S D, Pachon J H et al. 2010 IEEE Nuclear Science Symposium Conference Record, 2010. 2319